EXTENDED PDF FORMAT
SPONSORED BY
IMMUNOLOGY2013™ Travel Grants
from R&D Systems
$1000 travel grants will be awarded to 10 immunology researchers
Apply Now!
www.rndsystems.com

High-Resolution View of the Yeast Meiotic Program Revealed by Ribosome Profiling

Gloria A. Brar *et al.*

Science **335**, 552 (2012);
DOI: 10.1126/science.1215110

This copy is for your personal, non-commercial use only.

If you wish to distribute this article to others, you can order high-quality copies for your colleagues, clients, or customers by clicking here.

Permission to republish or repurpose articles or portions of articles can be obtained by following the guidelines here.

The following resources related to this article are available online at www.sciencemag.org (this information is current as of January 10, 2013):

Updated information and services, including high-resolution figures, can be found in the online version of this article at:
http://www.sciencemag.org/content/335/6068/552.full.html

Supporting Online Material can be found at:
http://www.sciencemag.org/content/suppl/2011/12/21/science.1215110.DC1.html

This article **cites 57 articles**, 24 of which can be accessed free:
http://www.sciencemag.org/content/335/6068/552.full.html#ref-list-1

This article has been **cited by** 11 articles hosted by HighWire Press; see:
http://www.sciencemag.org/content/335/6068/552.full.html#related-urls

This article appears in the following **subject collections:**
Cell Biology
http://www.sciencemag.org/cgi/collection/cell_biol

Downloaded from www.sciencemag.org on January 10, 2013

Science (print ISSN 0036-8075; online ISSN 1095-9203) is published weekly, except the last week in December, by the American Association for the Advancement of Science, 1200 New York Avenue NW, Washington, DC 20005. Copyright 2012 by the American Association for the Advancement of Science; all rights reserved. The title *Science* is a registered trademark of AAAS.

High-Resolution View of the Yeast Meiotic Program Revealed by Ribosome Profiling

Gloria A. Brar,[1] Moran Yassour,[2,3,4] Nir Friedman,[4,5] Aviv Regev,[2,3] Nicholas T. Ingolia,[1]*† Jonathan S. Weissman[1]†

Meiosis is a complex developmental process that generates haploid cells from diploid progenitors. We measured messenger RNA (mRNA) abundance and protein production through the yeast meiotic sporulation program and found strong, stage-specific expression for most genes, achieved through control of both mRNA levels and translational efficiency. Monitoring of protein production timing revealed uncharacterized recombination factors and extensive organellar remodeling. Meiotic translation is also shifted toward noncanonical sites, including short open reading frames (ORFs) on unannnotated transcripts and upstream regions of known transcripts (uORFs). Ribosome occupancy at near-cognate uORFs was associated with more efficient ORF translation; by contrast, some AUG uORFs, often exposed by regulated 5′ leader extensions, acted competitively. This work reveals pervasive translational control in meiosis and helps to illuminate the molecular basis of the broad restructuring of meiotic cells.

Sexual reproduction is enabled by meiosis, a strongly conserved cell division that generates haploid progeny from a diploid precursor. Meiosis has been studied for over a century, including extensive analyses in the budding yeast *Saccharomyces cerevisiae* [reviewed in (*1*, *2*)], where it is linked to spore formation. These efforts have provided a wealth of knowledge about the movement and changes in organization of meiotic chromosomes. Far less is known about the molecular basis of the remodeling events that have an impact on other aspects of meiotic cellular physiology. Pioneering microarray studies (*3*) provided a basic framework of molecular changes accompanying yeast meiotic progression but failed to capture many dynamic processes, in part because of extensive posttranscriptional regulation, including specific instances of functionally significant translational control [reviewed in (*2*); see also (*4*)]. Whether translational control plays a general role in meiotic protein production, however, is unclear.

Ribosome profiling, based on deep sequencing of ribosome-protected mRNA fragments, allows monitoring of translation with scale, speed, and accuracy that rivals approaches for following mRNA levels (*5*, *6*). Applying this method to sporulating *S. cerevisiae* cells allowed us to follow the molecular events underlying meiosis with unprecedented depth.

A high-resolution atlas of meiotic mRNA abundance and new protein synthesis. Our studies relied on three critical features: optimized meiotic synchrony, dense time points that oversampled meiotic transitions, and in-depth staging of each time point. We collected samples through two separate meiosis experiments (Fig. 1, A and B, and fig. S1A). The first used an optimized version of traditional synchronization procedures and focused on early meiotic stages. The second time course used an estrogen-activatable derivative of the Ndt80 transcription factor (*4*, *7*), which allowed synchronous progression through the meiosis I and II (MI and MII) chromosome segregation stages (*4*). Each time point was staged in detail (Fig. 1B and figs. S2 and S3), and we selected 25 of them, chosen for comprehensive meiotic coverage, along with two cycling vegetative samples, for ribosome profiling and mRNA sequencing (Fig. 1A and fig. S1A). Use of time points that oversampled meiotic stages allowed for synthesis of the data into a master time course (Fig. 1A and fig. S1B) and selective pooling, which collapsed meiotic progression into nine categories for some analyses (fig. S4).

Staging revealed a high degree of synchrony and provided a cytological framework to anchor expression data (Fig. 1B and figs. S2 and S3). Examination of ribosome footprints for specific genes showed that the sample synchrony was reflected in sharp, discrete translation patterns (Fig. 1C). The large majority (6134 out of 6708) of genes were translated at some point in meiosis, and most showed strong temporal regulation. In addition to a large shift in expression patterns between vegetative cells and cells entering meiosis, 66% of meiotically expressed genes varied by at least 10-fold in protein synthesis level through meiotic progression itself, a range that far exceeded measurement errors (Fig. 2A and fig. S5, A to D). These changes were due largely to the meiotic program itself rather than the nutrient deprivation conditions that accompany sporulation (fig. S6).

Expression clustering to probe meiotic cell biology and gene function. Clustering of the time points by genome-wide protein synthesis patterns precisely recapitulated their order (figs. S1B and S6A). Thus, dynamic control of protein synthesis results in unique expression signatures throughout the meiotic program. Accordingly, grouping of all genes by protein synthesis pattern through meiosis revealed numerous multifaceted clusters (Fig. 2A).

Many clusters emerged from groups of functionally related genes. This was seen prominently for genes involved in translation, mitochondrial function, mitochondrial translation, nutrient uptake, proteasome function, and redox reactions (Fig. 2A, numbered in the middle panel, and tables S1 and S2). Furthermore, a tight cluster of 27 proteins that were synthesized at the onset of DNA replication was predominantly composed of critical DNA replication and chromosome structure factors [Fig. 2A, top, and table S2; (*8*)]. Similarly, genes involved in recombination and synaptonemal complex (SC) formation were expressed precisely when these processes occurred, and they emerged as a discrete group containing 46 genes from unbiased clustering of the full data set (Fig. 2A, bottom, and table S2). Notably, this cluster included the large majority of meiotic genes with characterized roles in double-strand–break formation, crossover-noncrossover choice, and SC structure [reviewed in (*9*–*11*)].

Several uncharacterized genes were found in the recombination and SC cluster, which suggested that they are involved in these intensely studied processes (*1*). Indeed, loss of either *YDR506C* or *YLR445W* delayed nuclear division, consistent with a role for these factors in prophase, when recombination and SC formation occur (Fig. 2, B and C, and fig. S7A). *ydr506c*Δ and *ylr445w*Δ cells showed distinct, specific defects in SC morphogenesis (fig. S7, B and C), and in both cases, the meiotic progression delay was largely alleviated when the recombination checkpoint was bypassed by deletion of *SPO11* (Fig. 2, B and C, and fig. S7A). The strong delay in *ylr445w*Δ cells, however, was not fully dependent on Spo11 (Fig. 2C and fig. S7A), which implied that this gene has additional functions.

Evidence for cellular remodeling. Whereas our ability to observe precise temporal regulation allowed specific coclustering of some genes, there were prominent cases in which genes with a common function or localization showed highly disparate expression patterns. For example, we found tightly controlled but distinct patterns of expression among endoplasmic reticulum (ER) proteins, which suggested major ER remodeling events (fig. S8 and table S3). A strong down-regulation (relative to vegetative cells) of a set of ER genes, including

[1]Howard Hughes Medical Institute, Department of Cellular and Molecular Pharmacology, University of California, San Francisco, and California Institute for Quantitative Biosciences, San Francisco, CA 94158, USA. [2]Broad Institute of Massachusetts Institute of Technology and Harvard, Cambridge, MA 02142, USA. [3]Howard Hughes Medical Institute, Department of Biology, Massachusetts Institute of Technology, Cambridge, MA 02139, USA. [4]School of Engineering and Computer Science, Hebrew University, Jerusalem 91904, Israel. [5]Alexander Silberman Institute of Life Sciences, Hebrew University, Jerusalem 91904, Israel.

*Present address: Department of Embryology, Carnegie Institution for Science, Baltimore, MD 21218, USA.

†To whom correspondence should be addressed. E-mail: ingolia@ciwemb.edu (N.T.I.); weissman@cmp.ucsf.edu (J.S.W.)

Downloaded from www.sciencemag.org on January 10, 2013

ergosterol biosynthesis components, occurred before meiotic induction. After meiotic entry, a broad group of ER genes was induced, including glycosylation factors (table S3). Finally, after MI, a subset of folding factors, sphingolipid biosynthetic genes, and trafficking components were up-regulated. This last remodeling phase is accompanied by induction of the unfolded protein response (UPR) (*12*, *13*) (Fig. 1C, see also Fig. 3F below).

Autophagy components also showed discrete patterns of expression, which suggested dynamic control of distinct autophagic processes during sporulation [fig. S9A and table S4; (*14*)]. *ATG8*, a gene central to many branches of autophagy (*15*), was highly expressed from early in the meiotic program, and its deletion caused an early and profound meiotic defect (fig. S9, B and C). By contrast, *ATG32*, a mitophagy-specific factor (*16*, *17*), showed low expression until the meiotic divisions (fig. S9B). Delayed onset of mitophagy may ensure full mitochondrial function, which is needed to power early meiotic stages (*18*). Consistently, *atg32*Δ cells progressed normally past prophase but showed delayed meiotic completion (fig. S9D).

Translational control in meiosis. Control of protein production reflects both regulation of mRNA levels and the efficiency with which these messages are translated into proteins. Measuring translation rates and mRNA levels allowed us to evaluate their relative contributions. Much transcriptional regulation was observed, but translational control also regulated the magnitude and timing of protein production in meiotic cells. An example of this interplay is provided by the adjacent *SPS1* and *SPS2* genes (Fig. 3A). mRNA for both genes accumulated late in prophase and persisted through the meiotic divisions, consistent with their transcriptional control by *NDT80* (*19*). By contrast, *SPS1*, but not *SPS2*, was strongly translationally regulated, which resulted in delayed Sps1 protein synthesis until MII (Fig. 3, A and B).

To quantitatively evaluate the role of translational control, we calculated relative translation efficiencies [TEs; ribosome footprint RPKM/mRNA RPKM; where RPKM is reads per kilobase of coding sequence per million mapped reads, as in (*6*)] for messages across our time course. Replicates indicated high TE reproducibility (error <20%), which allowed sensitive measurement of dynamic translational control [fig. S5, E and F; (*6*)]. This approach confirmed, both in timing and degree, the strong MI-specific translational repression that regulates the B-type cyclin, *CLB3* [(*4*), Fig. 3C]. At least 10 genes showed a pattern of translational regulation highly similar to that of *CLB3*—including *SPS1* (Fig. 3A), *GIP1*, and *SPO20*—which, like *CLB3*, have known roles only late in meiosis (*20*–*22*).

Genome-wide analysis revealed that meiotic translational regulation is both pervasive and nuanced (Fig. 3D). As seen for vegetative cells (*6*), meiotic cells showed strong basal differences in translation rates among genes (Fig. 3D). Globally, we observed a net decrease in translation, relative to vegetative cells in their exponential growth phase, that was most pronounced at the very earliest and latest time points (fig. S10). Further, gene-specific translational regulation was widely used to dynamically tune gene expression. For example, 24% of genes during the "core meiotic" period showed greater than threefold TE changes, a period during which net translation capacity appears stable (fig. S10). More than 200 genes in the full time course and 66 in the core meiotic period exhibited a dynamic range in TE that was comparable to the ~10-fold changes seen for *GCN4*, an archetype of strong translational regulation (*23*).

Changes in TE frequently correlated with timing of gene function (Fig. 3E). The DNA replication factor *ORC1* (*24*), for example, showed strong translational repression at later meiotic stages when cells do not replicate DNA. Zip1, an SC component (*25*), specifically showed poor translation in vegetative cells and spores, consistent with the lack of SC in either state. Chitin deposition factor Rcr1 (*26*) is translated efficiently only at late time points, concomitant with new cell wall generation. Finally, *HAC1*, the central UPR mediator (*12*, *13*), showed transient translational activation shortly upon transfer of cells to nutrient-limited conditions, followed by a later, stronger translational activation

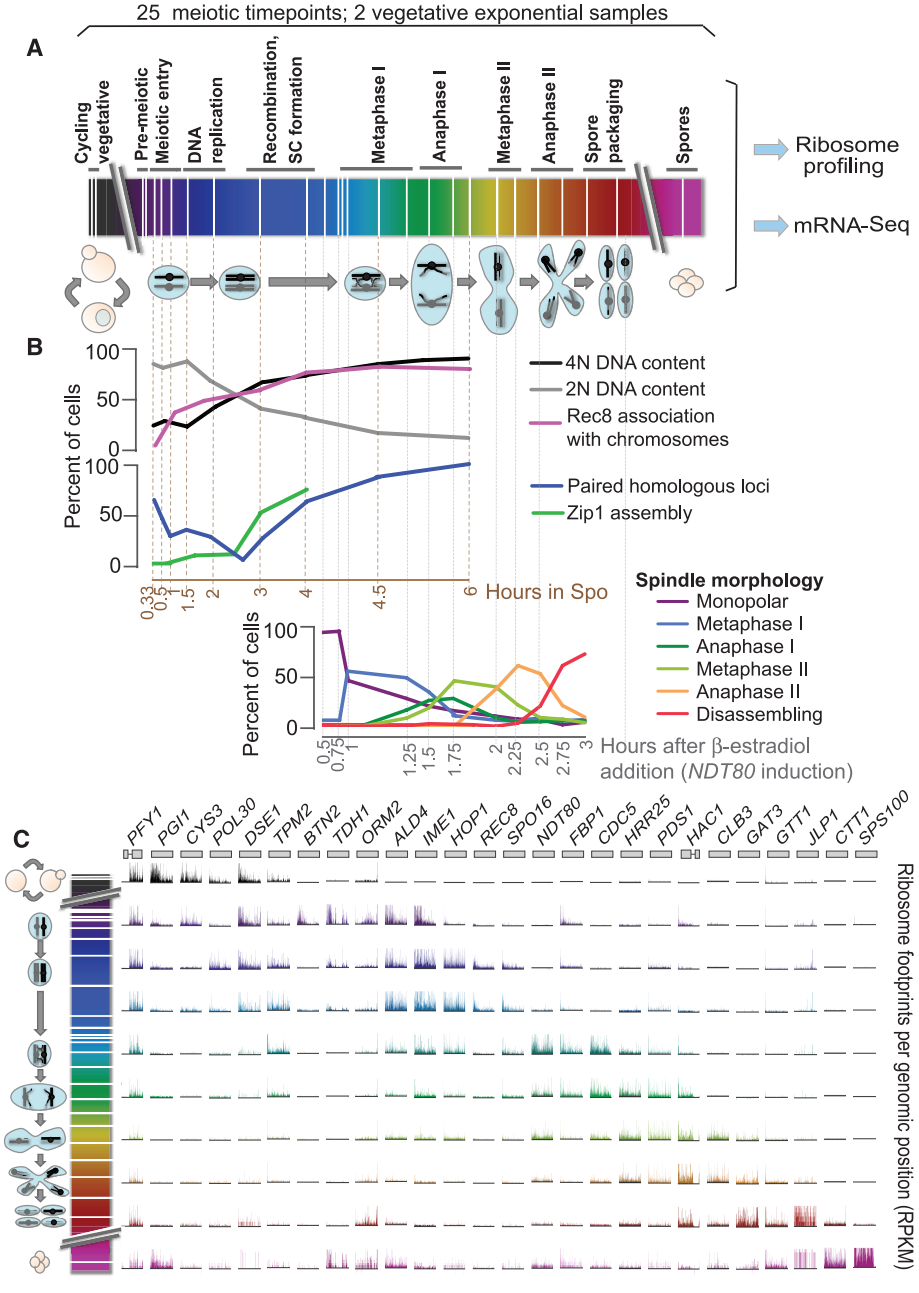

Fig. 1. Ribosome profiling through meiosis. (**A**) Time points (white lines) were taken through two overlapping time courses. Cartoon representations of meiotic stages are below. (**B**) A subset of staging controls. Positions of staging plots correspond to time points in (A). (**C**) Ribosome footprints across specific genes are shown for categories in fig. S4. Scales on the *y* axis are independent by gene.

Downloaded from www.sciencemag.org on January 10, 2013

during the meiotic divisions, as cells are synthesizing new membrane and spore walls (Fig. 3F). *HAC1* is regulated translationally through cytoplasmic splicing of its message (*27*). Consistently, *HAC1* mRNA splicing mirrored TE measurements, both in timing and degree (Fig. 3F). The UPR has been heavily studied in yeast using harsh inhibitors of ER folding (e.g., dithiothreitol). This study reveals a novel physiological setting to follow UPR induction.

Noncanonical translation. Beyond translational control of canonical open reading frames (ORFs), we also observed a shift toward noncanonical translation during the meiotic program. Whereas vegetative cells exhibited ~5% of ribosome footprints mapping outside annotated ORFs, in meiotic cells, up to ~30% of footprints mapped outside of these regions (Fig. 4A). These footprints largely mapped to discrete novel translation sites with well-defined AUG starts and stop codon stops. We systematically annotated translation units by exploiting the strong peak in ribosome density seen at translation initiation sites to identify utilized start codons [fig. S11, (*6*)]. This strategy was sensitive, which allowed de novo identification of start codons for most known ORFs (fig. S12A) and specific, strongly enriching for ORFs initiating at AUG (fig. S13).

Novel ORFs were found on noncanonical mRNAs, including transcripts antisense to known ORFs, alternate transcripts at canonical loci, and transcripts in regions thought to be intergenic (Fig. 4, B and C, and figs. S12A, S14, and S15A). We also identified instances of genome misannotation (e.g., fig. S15B). Many newly annotated ORFs were on stable transcripts, similar to those predicted as noncoding in a meiotic tiling array study [(*28*), fig. S14]. Our empirical strategy found translation of short ORFs (sORFs) (fig. S12A) that were well-expressed (fig. S12, B and C) and highly regulated (fig. S16) but below the cutoff of 80 to 100 amino acids used historically to computationally identify yeast ORFs.

Recent studies have identified cellular functions for short peptides (*29*, *30*), although the function of these meiotic sORFs remains an open question. Minimally, our data suggest the export of many novel transcripts into the cytoplasm, allowing translation by ribosomes. Conversely, this data set facilitates identification of transcripts that act at the RNA level. For example, most antisense transcripts are poorly translated, including *RME2* and *RME3* (antisense to *IME4* and *ZIP2*, respectively), which are known to act through direct cis-transcriptional interference of their sense counterpart [figs. S12C and S17, A, B, and D; (*31*, *32*)]. By contrast, a transcript antisense to *YFL012W* that shows no transcriptional interference activity contained prominent regions of translation [(*31*), fig. S17, C and D].

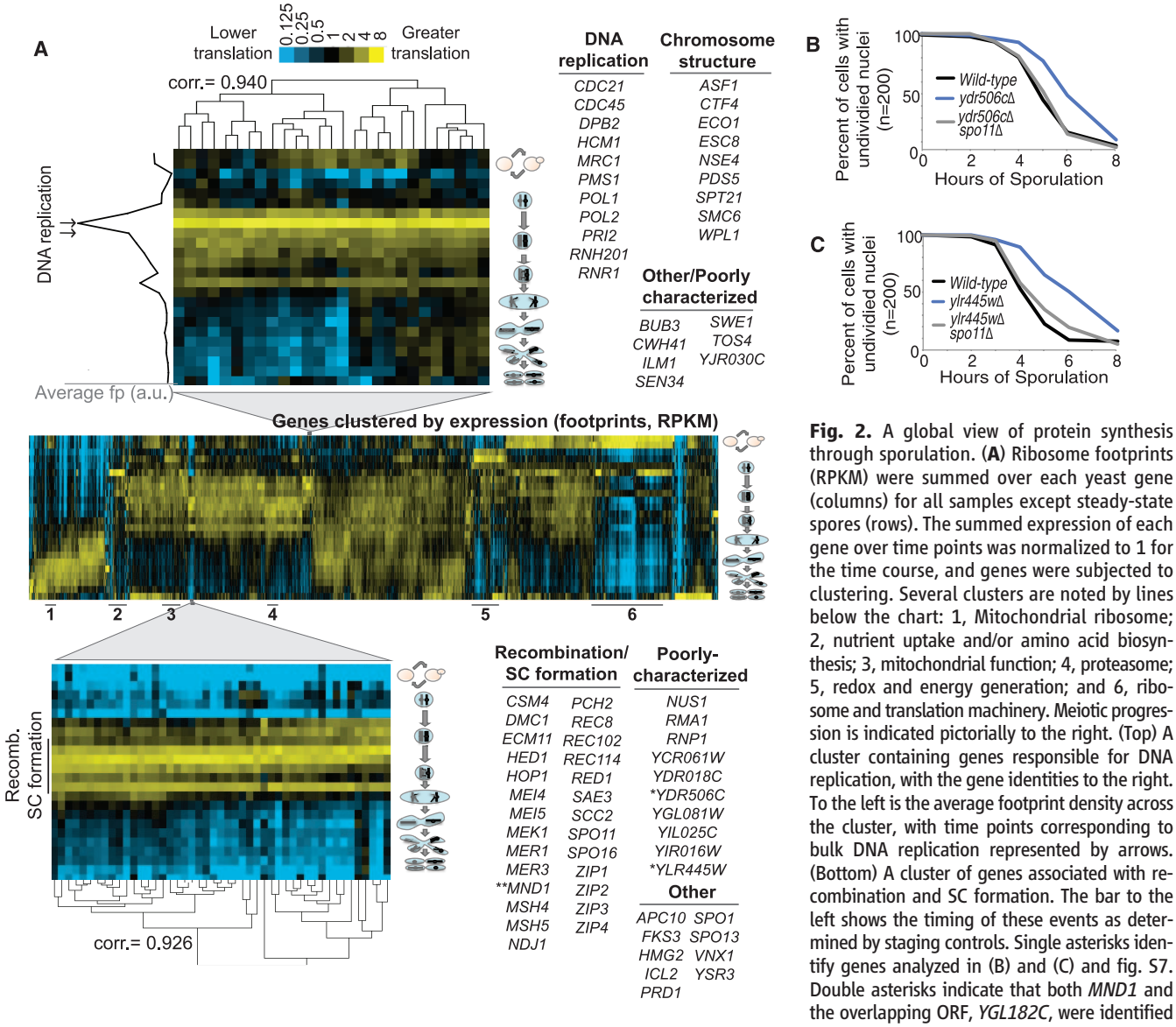

Fig. 2. A global view of protein synthesis through sporulation. (**A**) Ribosome footprints (RPKM) were summed over each yeast gene (columns) for all samples except steady-state spores (rows). The summed expression of each gene over time points was normalized to 1 for the time course, and genes were subjected to clustering. Several clusters are noted by lines below the chart: 1, Mitochondrial ribosome; 2, nutrient uptake and/or amino acid biosynthesis; 3, mitochondrial function; 4, proteasome; 5, redox and energy generation; and 6, ribosome and translation machinery. Meiotic progression is indicated pictorially to the right. (Top) A cluster containing genes responsible for DNA replication, with the gene identities to the right. To the left is the average footprint density across the cluster, with time points corresponding to bulk DNA replication represented by arrows. (Bottom) A cluster of genes associated with recombination and SC formation. The bar to the left shows the timing of these events as determined by staging controls. Single asterisks identify genes analyzed in (B) and (C) and fig. S7. Double asterisks indicate that both *MND1* and the overlapping ORF, *YGL182C*, were identified in this cluster. (**B**) Wild-type, *ydr506c*Δ, and *ydr506c*Δ*spo11*Δ cells were induced to sporulate. At indicated times, samples were scored for nuclear division. (**C**) Wild-type, *ylr445w*Δ, and *ylr445w*Δ *spo11*Δ cells were induced to sporulate and were treated as in (B).

Downloaded from www.sciencemag.org on January 10, 2013

uORFs in meiosis. The second major source of novel meiotic ribosome density was leader sequences [commonly called 5′ untranslated regions (5′UTRs)], situated upstream of canonical ORFs (Fig. 4D and fig. S18A). We saw no general meiotic increase in footprints in 3′UTRs, which argues against a non-specific increase in translational background noise. Examination of individual gene leaders revealed short footprint spans that started at either AUGs or near-cognate codons and generally spanned the region until the next stop codon (Fig. 4D and fig. S18A). Nearly 300 of such upstream ORFs (uORFs) have been identified in yeast under starvation conditions [(*6*), reviewed in (*33*)], but we found them to be far more common in meiosis.

We annotated 10,226 meiotic uORFs, present in the leaders of 3026 genes (fig. S11). These uORFs contained a density of ribosome footprints far greater than the ribosome footprint density in non-uORF leader regions, which suggested that our annotation approach was thorough and specific (fig. S19, A and B). Ribosome occupancy at uORFs was higher in meiotic than vegetative cells (Fig. 4D and figs. S18A and S19, B and C), and most of this effect derives from the meiotic program itself rather than the starvation conditions that accompany sporulation (fig. S19D). As expected, AUG, when present, was efficiently used for uORF translation initiation. The near-cognate codons that showed most efficient initiation, UUG and CUG (fig. S18, B and C), have also been shown to be most efficient in mammalian cells and in vitro (*5*, *34*).

uORFs have been implicated in translational regulation, although no universal functional role has emerged. uORFs that have been well-characterized through reporter studies show diverse effects: enhancing, decreasing, or having little impact on downstream ORF translation [reviewed in (*33*)]. Three features of our study ideally positioned us to evaluate the role of uORFs in translation. First, we annotated many uORFs, which allowed us to distill general principles. Second, we collected data for each time point on mRNA abundance and rates of translation, which provided instantaneous quantification of TE for each downstream ORF, whereas traditional approaches require TE inference by steady-state protein abundance. Finally, our analysis of numerous sequential points through a dynamic process permitted us to detect temporal trends. Comparison of ribosome occupancy of leaders and TE of their corresponding downstream ORFs over 10 time points (see fig. S4) typically revealed a strong positive correlation (Fig. 4, E and F). However, a subset of leaders containing at least one AUG uORF showed a negative correlation, which suggested competition between uORF and ORF translation in these cases (Fig. 4F and fig. S20; see Fig. 5E below).

Leader extensions and competitive uORFs. For some messages, we found that enriched footprint occupancy of leaders was caused by a programmed change in the transcript length during meiosis. Systematic analysis identified 192 genes with regulated leader length (Fig. 5, A to C; fig. S21; and table S5). For example, *ORC1* showed an extended leader after prophase. This extension revealed a number of well-translated uORFs (Fig. 5B) and was accompanied by a concurrent decrease in translation of the *ORC1* coding region (Figs. 3E and 5, B and D). Of genes with regulated leaders, a prominent subset showed a similar negative correlation, often corresponding well with known gene function. Orc1 and Ndj1, for example, have no characterized function late in meiosis (*24*, *35*), and *RED1*, a key meiotic prophase factor (*36*), is translationally repressed exclusively in vegetative cells (Fig. 5D).

For genes with leader extensions containing one or more AUG uORF, at least half showed a strong negative correlation between the ribosome occupancy of the leader and TE of the ORF (Fig. 5E). By contrast, for leaders containing uORFs starting only with near-cognate, non-AUG codons, this correlation was strongly positive (Fig. 5E). Regulated leaders have been observed in budding yeast and mammalian cells, with longer forms often associated with poor ORF translation (*37*, *38*). Here, we have observed a far broader and more nuanced role for leader extensions in providing temporal translational control to many meiotic genes.

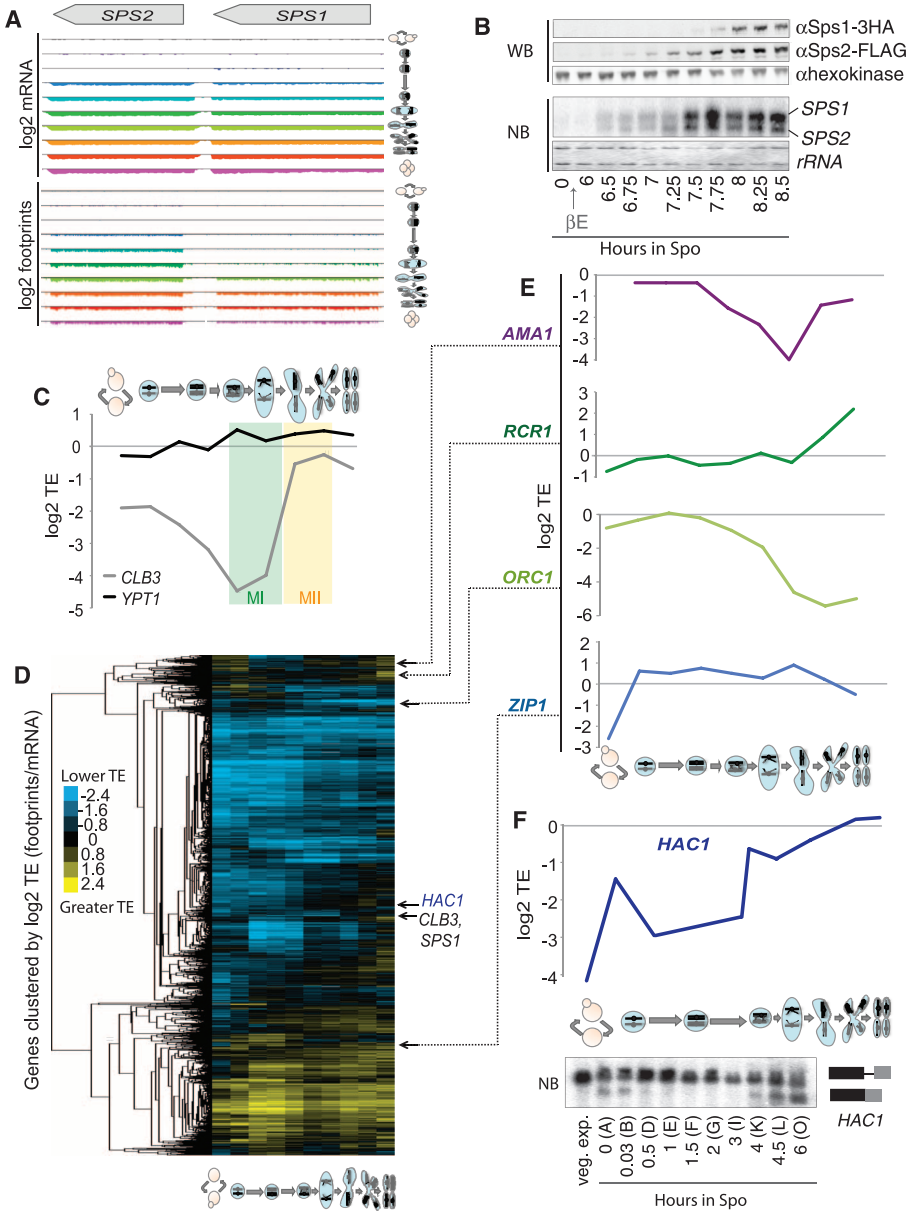

Fig. 3. Widespread dynamic translational control in meiosis. (**A**) Log_2 mRNA and footprints (RPKM) for a region containing *SPS1* and *SPS2* over pooled time points (fig. S4). (**B**) *SPS1-3HA* and *SPS2-FLAG* cells carrying an estrogen-inducible *NDT80* allele were induced to sporulate. At 6 hours, β-estradiol was added. Samples from indicated times were subjected to Western blotting (WB) and Northern blotting (NB). (**C**) Log_2 TE values for *CLB3* and *YPT1* for pooled time points (fig. S4). MI and MII are indicated by colored shading as boxes. (**D**) Cluster analysis of log_2 TE through meiosis for pooled categories (fig. S4) for all genes. (**E**) Log_2 TEs are plotted as in (C) for *AMA1*, *RCR1*, *ORC1*, and *ZIP1*. (**F**) Log_2 TEs are plotted as in (C) for *HAC1*. Below, total RNA from the original time course (see fig. S1) was subjected to Northern blotting for *HAC1*.

Downloaded from www.sciencemag.org on January 10, 2013

More generally, our analyses point to disparate roles for AUG and near-cognate uORFs (Figs. 4F and 5E). A fraction of AUG uORFs appear to competitively down-modulate ORF expression. By contrast, near-cognate uORFs are more common and show a generally strong positive correlation with expression of their downstream ORF, which may allow cells to divert limited resources to an important subset of messages. Whether uORFs directly prime translation of their downstream ORF is unclear. Nonetheless, genes with the strongest positive correlation between leader ribosome occupancy and ORF TE are highly enriched for known function in sporulation (table S6), which suggests physiological relevance of this regulation. The broad monitoring of gene expression by genomics has underscored the importance of quantitative modulation, beyond a model of binary on-off control. MicroRNAs provide a prominent example of developmental control through subtle regulation of broad sets of genes. uORFs may similarly allow condition-specific tuning of protein synthesis for a large portion of the genome.

The preponderance of uORFs suggests a shift of the translation initiation mechanism in meiotic cells from the predominant mechanism in which initiation factors recognize the mRNA cap and the initiation complex scans the message for the first AUG to commence translation [reviewed in (*23*)]. A link between alternative translation initiation mechanisms and the use of uORFs is suggested by analysis of messages that were shown to support cap-independent translation in nitrogen-starved yeast cells (*YMR181C*, *GPR1*, *BOI1*, *FLO8*, *NCE102*, *MSN1*, and *GIC1*) (*39*). We found that all had leaders with well-translated near-cognate uORFs and a strong positive correlation between leader ribosome occupancy and ORF translation (Fig. 4F; fig. S22, excluding *BOI1* as it has a complicating leader extension; table S5).

Perspective. We find that even in the extensively studied yeast, *S. cerevisiae*, genome coding has a complexity not captured by existing annotations. Ribosome profiling also captured a layer of regulation that is invisible to mRNA measurements alone and which revealed extensive and dynamic translational regulation of canonical ORFs. Transcription studies have enabled the identification of cis- and trans-transcriptional elements that control diverse cellular processes, whereas a similarly broad understanding of the importance and mechanisms of translational control remains elusive. This data set provides a valuable foundation for identifying such cis- and trans-translational regulators.

This study also gives a holistic view of the metabolic and cellular reorganization seen through the yeast meiotic program that extends beyond a traditional chromosome-centric picture. Previous studies suggested that meiotic transcriptional control was limited to a few discrete waves (*3*, *40*). Our data reveal multifaceted control of protein production, enabled by the tightly timed induction of many translational and transcriptional programs, including those driving translation factors, the proteasome, and the UPR. Indeed, the view of such responses as environmentally controlled stress pathways may reflect the historical context of their discovery rather than their sole physiological role.

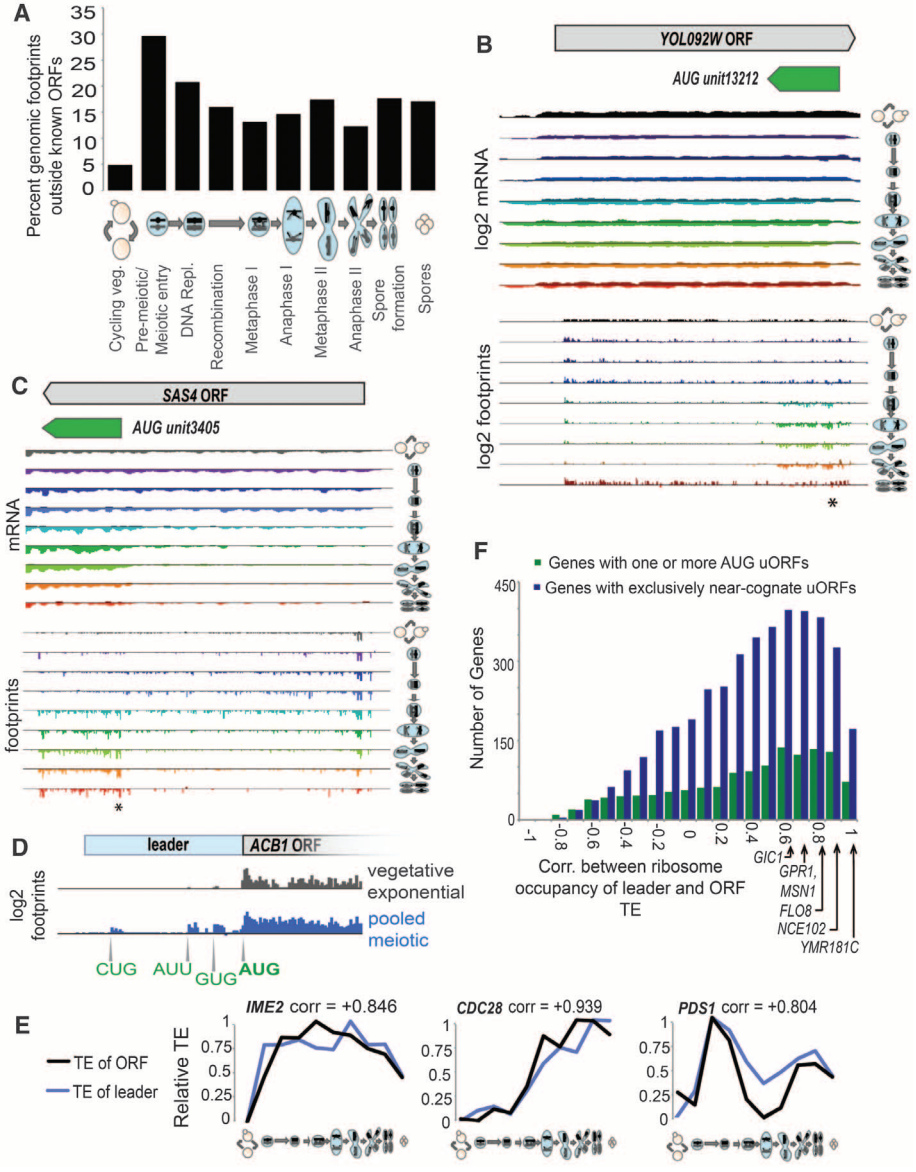

Fig. 4. Noncanonical translation is pervasive in meiotic cells. (**A**) Footprints from pooled time points (see fig. S4) were mapped. The percentage of these footprints outside of known ORF annotations is plotted. (**B**) mRNA and ribosome occupancy profiles around *YOL092W*, with sense above the line for each time point and antisense below. Single asterisk denotes the sORF start site. The "AUG unit" (sORF) was annotated by the strategy shown in fig. S11. (**C**) The region around *SAS4* is displayed as in (B), with truncated ORF start denoted by a single asterisk. (**D**) Ribosome occupancy profile for vegetative cells in exponential growth phase and meiotic cells over the leader of *ACB1*. (**E**) For pooled time points (see fig. S4), TEs are plotted for ORFs and for leaders (see SOM for a discussion of leader TE determination) for *IME2*, *CDC28*, and *PDS1*. Values are normalized to the same range for both plots. (**F**) Correlation coefficients [determined from plots as in (E)] were determined for each gene with uORFs for leaders with only near-cognate uORFs and at least one AUG uORF. The positions of six genes that support cap-independent translation (*39*) are noted.

References and Notes

1. D. Zickler, N. Kleckner, *Annu. Rev. Genet.* **33**, 603 (1999).
2. A. L. Marston, A. Amon, *Nat. Rev. Mol. Cell Biol.* **5**, 983 (2004).
3. S. Chu *et al.*, *Science* **282**, 699 (1998).
4. T. M. Carlile, A. Amon, *Cell* **133**, 280 (2008).
5. N. T. Ingolia *et al.*, *Cell* **147**, 789 (2011).
6. N. T. Ingolia *et al.*, *Science* **324**, 218 (2009).
7. K. R. Benjamin, C. Zhang, K. M. Shokat, I. Herskowitz, *Genes Dev.* **17**, 1524 (2003).
8. P. T. Spellman *et al.*, *Mol. Biol. Cell* **9**, 3273 (1998).
9. A. Lynn *et al.*, *Chromosome Res.* **15**, 591 (2007).
10. S. Keeney, M. J. Neale, *Biochem. Soc. Trans.* **34**, 523 (2006).
11. S. L. Page, R. S. Hawley, *Annu. Rev. Cell Dev. Biol.* **20**, 525 (2004).
12. J. S. Cox, P. Walter, *Cell* **87**, 391 (1996).
13. K. Mori *et al.*, *Genes Cells* **1**, 803 (1996).

Note added in proof: YDR506C and *YLR445W* are now named *GMC1* and *GMC2*, respectively.

Downloaded from www.sciencemag.org on January 10, 2013

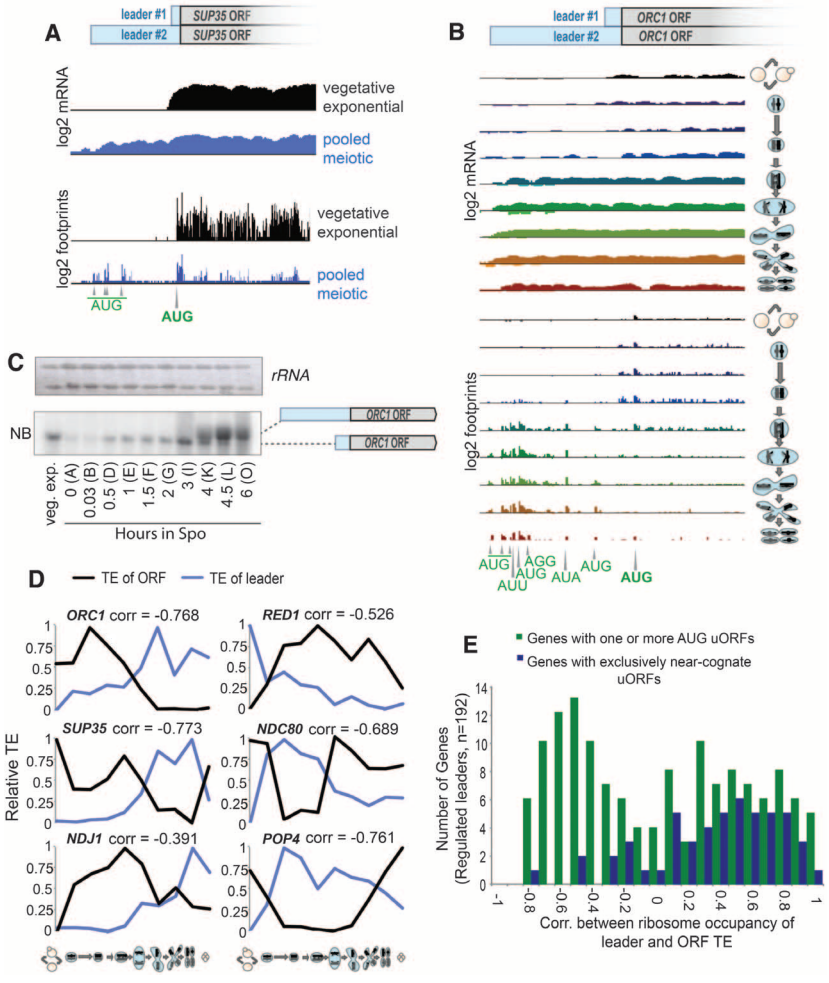

Fig. 5. Regulated transcript extensions expose novel regulatory uORFs. (**A**) mRNA and ribosome occupancy profiles around *SUP35*. (**B**) *ORC1* region displayed as in Fig. 4B. (**C**) Total RNA from the original time course (see fig. S1) was subjected to Northern blotting (NB) for *ORC1*. (**D**) Analysis as in Fig. 4E for *ORC1*, *SUP35*, *NDJ1*, *RED1*, *NDC80*, and *POP4*. (**E**) Analysis as in Fig. 4F for genes with regulated leader extension (table S5).

14. I. Piekarska *et al.*, *Eur. J. Cell Biol.* **89**, 780 (2010).
15. Z. Xie, D. J. Klionsky, *Nat. Cell Biol.* **9**, 1102 (2007).
16. T. Kanki *et al.*, *Dev. Cell* **17**, 98 (2009).
17. K. Okamoto *et al.*, *Dev. Cell* **17**, 87 (2009).
18. A. Jambhekar, A. Amon, *Curr. Biol.* **18**, 969 (2008).
19. S. Chu, I. Herskowitz, *Mol. Cell* **1**, 685 (1998).
20. A. M. Neiman, *J. Cell Biol.* **140**, 29 (1998).
21. H. Tachikawa *et al.*, *J. Cell Biol.* **155**, 797 (2001).
22. H. Friesen *et al.*, *Genes Dev.* **8**, 2162 (1994).
23. N. Sonenberg, A. G. Hinnebusch, *Cell* **136**, 731 (2009).
24. S. P. Bell *et al.*, *Science* **262**, 1844 (1993).
25. M. Sym *et al.*, *Cell* **72**, 365 (1993).
26. K. Imai *et al.*, *J. Biol. Chem.* **280**, 8275 (2005).
27. C. Sidrauski, J. S. Cox, P. Walter, *Cell* **87**, 405 (1996).
28. A. Lardenois *et al.*, *Proc. Natl. Acad. Sci. U.S.A.* **108**, 1058 (2011).
29. T. Kondo *et al.*, *Science* **329**, 336 (2010).
30. Y. Xu, D. Ganem, *J. Virol.* **84**, 5465 (2010).
31. B. Gelfand *et al.*, *Mol. Cell. Biol.* **31**, 1701 (2011).
32. C. F. Hongay *et al.*, *Cell* **127**, 735 (2006).
33. H. M. Hood *et al.*, *Annu. Rev. Microbiol.* **63**, 385 (2009).
34. S. E. Kolitz, J. E. Takacs, J. R. Lorsch, *RNA* **15**, 138 (2009).
35. H. Y. Wu, S. M. Burgess, *Curr. Biol.* **16**, 2473 (2006).
36. B. Rockmill, G. S. Roeder, *Proc. Natl. Acad. Sci. U.S.A.* **85**, 6057 (1988).
37. J. Badhai *et al.*, *PLoS ONE* **6**, e17672 (2011).
38. G. L. Law *et al.*, *Genome Biol.* **6**, R111 (2005).
39. W. V. Gilbert *et al.*, *Science* **317**, 1224 (2007).
40. A. P. Mitchell, *Microbiol. Rev.* **58**, 56 (1994).

Acknowledgments: We thank E. Ünal, A. Amon, and members of the Weissman laboratory for critical reading of this manuscript; C. Chu for sequencing assistance; J. Dunn for protocol development assistance; F. Van Werven for the MATa/a strain; and F. Klein for the the Zip1 antibody. G.A.B. is supported by American Cancer Society Postdoctoral Fellowship 117945-PF-09-136-01-RMC. M.Y. is supported by a Clore Fellowship. This work was supported by a grant from the U.S.-Israel Binational Science Foundation (N.F. and A.R.), an NIH P01 award (AG10770; N.T.I.), a Ruth L. Kirschstein National Research Service Award (GM080853; N.T.I.), and Howard Hughes Medical Institute funding (J.S.W. and A.R.). A patent on the ribosome profiling approach has been assigned to the University of California. Supporting files are in the SOM and at www.ncbi.nlm.nih.gov/geo/ with series accession no. GSE34082.

Supporting Online Material

www.sciencemag.org/cgi/content/full/science.1215110/DC1
Materials and Methods
Figs. S1 to S22
Tables S1 to S7
References (*41*–*57*)
Files S1 and S2

11 October 2011; accepted 13 December 2011
Published online 22 December 2011;
10.1126/science.1215110

Downloaded from www.sciencemag.org on January 10, 2013

The Southern Ocean's Role in Carbon Exchange During the Last Deglaciation

Andrea Burke[1,2]* and Laura F. Robinson[2,3]

Changes in the upwelling and degassing of carbon from the Southern Ocean form one of the leading hypotheses for the cause of glacial-interglacial changes in atmospheric carbon dioxide. We present a 25,000-year-long Southern Ocean radiocarbon record reconstructed from deep-sea corals, which shows radiocarbon-depleted waters during the glacial period and through the early deglaciation. This depletion and associated deep stratification disappeared by ~14.6 ka (thousand years ago), consistent with the transfer of carbon from the deep ocean to the surface ocean and atmosphere via a Southern Ocean ventilation event. Given this evidence for carbon exchange in the Southern Ocean, we show that existing deep-ocean radiocarbon records from the glacial period are sufficiently depleted to explain the ~190 per mil drop in atmospheric radiocarbon between ~17 and 14.5 ka.

The transition between the Last Glacial Maximum [LGM; ~22 to 18 ka (thousand years ago)] and the warm climate of the Holocene was accompanied by an ~80 parts per million rise in atmospheric CO_2 (*1*) and a substantial reduction in the ratio of radiocarbon (^{14}C) to ^{12}C in the atmosphere (*2*). Of particular interest is the large and rapid drop in atmospheric radiocarbon during the first pulse of CO_2 rise at the last deglaciation (*3*). One hypothesis that has been proposed to explain the rise in atmospheric CO_2 and the concurrent fall in atmospheric radiocarbon content is the "isolated reservoir" hypothesis, which calls for ventilation of a carbon-rich, radiocarbon-depleted water mass that was isolated from the atmosphere during the glacial period (*4*). Increased

[1]Massachusetts Institute of Technology/Woods Hole Oceanographic Institution Joint Program in Oceanography, Mailstop 24, Woods Hole, MA 02543, USA. [2]Department of Marine Chemistry and Geochemistry, Woods Hole Oceanographic Institution, Mailstop 25, Woods Hole, MA 02543, USA. [3]School of Earth Sciences, University of Bristol, Wills Memorial Building, Queen's Road, Bristol BS8 1RJ, UK.

*To whom correspondence should be addressed. E-mail: aburke@whoi.edu